JOURNAL OF Materials CHEMISTRY

Crystallization of hydrothermally treated TiO_2 pillars in pillared montmorillonite for improvement of the photocatalytic activity

Chihiro Ooka,*[a] Shigendo Akita,[a] Yoshiaki Ohashi,[a] Tatsuro Horiuchi,[b] Kenzi Suzuki,[b] Shin-ichi Komai,[c] Hisao Yoshida[c] and Tadashi Hattori[d]

[a]*Nagoya Municipal Industrial Research Institute, 3-4-41, Rokuban, Atsuta-ku, Nagoya, 456-0058 Japan. E-mail: ohoka@nmiri.city.nagoya.jp*
[b]*National Industrial Research Institute of Nagoya, 1-1, Hirate-cho, Kita-ku, Nagoya, 462-0057 Japan*
[c]*Department of Applied Chemistry, Graduate School of Engineering, Nagoya University, Furo-cho, Chikusa-ku, Nagoya, 464-8603 Japan*
[d]*Research Center for Advanced Waste and Emission Management, Nagoya University, Furo-cho, Chikusa-ku, Nagoya, 464-8603 Japan*

Received 22nd February 1999, Accepted 23rd August 1999

A novel pillared clay, *i.e.* pillared montmorillonite with crystallized TiO_2, has been developed as a highly active photocatalyst. The TiO_2 pillars in pillared montmorillonite were crystallized to anatase by hydrothermal treatment, while the porosity of the pillared clay was retained. The size of the crystallized TiO_2 pillars and the average pore diameter showed good agreement, and both sizes could be controlled in the range *ca.* 40–90 Å by changing the treatment conditions. The photocatalytic properties of the TiO_2 pillars were investigated in the degradation of trichloroethylene in water. The hydrothermal crystallization enhanced the catalytic activity both per unit weight of TiO_2 and per exposed unit surface area of TiO_2. The catalytic activity of the TiO_2 pillars was also enhanced by quantum-size effects: as the TiO_2 pillar size decreased, the pillared montmorillonites exhibited higher catalytic activity and showed larger blue-shifts in their UV absorption spectra.

Pillared clays have attracted much attention as a new type of porous material in which small particles of metal oxide are intercalated into the silicate layers of a clay.[1–4] Pillared clays have a structure in which parallel two-dimensional silicate layers of the clay are supported with small particles of metal oxide and micro- to meso-pores are formed. Because of this particular structure, pillared clays have been shown to have potential uses as adsorbents, catalysts and catalyst supports.[5–9]

TiO_2 pillared clays[10–14] are characterized by their oxide pillars, *i.e.* TiO_2, of a few nm in size. This led to an attempt to apply TiO_2 pillared clays in photocatalysis. TiO_2 pillared clays showed photocatalytic activity because of the small TiO_2 particles, and shape selectivity because of the pore structure.[15] TiO_2 pillars in pillared clays synthesized in past studies were generally amorphous or very poorly crystalline, which generally resulted in lower photocatalytic activity than is exhibited by TiO_2 anatase. Therefore the activity of TiO_2 pillared clays may be improved by crystallizing the TiO_2 pillars to the anatase form. Furthermore, amorphous TiO_2 generally shows easier elution of Ti^{4+} in acidic solution than crystallized TiO_2.

In this study, the crystallization of TiO_2 pillars was attempted by hydrothermal treatment of TiO_2 pillared montmorillonite, and the effects of the hydrothermal treatment on the photocatalytic activity of the pillared montmorillonite in the degradation of trichloroethylene, and on the durability of the TiO_2 pillars in acidic solution, were investigated.

Experimental

Synthesis of the samples

The hydrothermally treated and untreated TiO_2 pillared clays prepared and the raw clay used in this study are listed in Table 1. The untreated samples were prepared with the procedure reported by Yamanaka *et al.*[11] Titanium tetra-isopropoxide was added to vigorously stirred 1 M HCl solution. The molar ratio of HCl to the alkoxide was unity. The resulting slurry was peptized at 50 °C to give a clear TiO_2 sol with a pH of 0.5.

The raw clay used was sodium montmorillonite (Kunipia-F, Kunimine Industrial Company) with the structural formula $(Na_{0.35}K_{0.01}Ca_{0.02})(Si_{3.89}Al_{0.11})(Al_{1.60}Fe_{0.08}Mg_{0.32})$-$O_{10}(OH)_2 \cdot nH_2O$,[16] and the cation exchange capacity (CEC) was 1.2 meq g^{-1}.[16] The prepared TiO_2 sol was mixed with a 1 wt% aqueous suspension of the raw clay. In this mixed suspension, the molar ratio of TiO_2/raw clay was 13.3, and TiO_2/eq. of exchangeable cation in the raw clay; the pH of the suspension was 0.8. The suspension was stirred for 3 h at 50 °C. The product was centrifuged and washed with water several times to remove excess TiO_2 sol. The TiO_2 pillared clay thus obtained was dispersed in water again, and then hydrothermally treated in an autoclave. The treatment temperature and time ranges used were 200–250 °C and 1–24 h, respectively, from the results of preliminary experiments. The treated product was separated and washed with water by centrifugation, and then dried in air at room temperature. All samples, both untreated and hydrothermally treated, were typically calcined at 500 °C. The TiO_2 pillared clay hydrothermally treated, for example, at 200 °C for 24 h will be referred to as HT(200, 24), and the untreated clay as UT. For the UT clay two batches of samples, UT-1 and UT-2, were prepared, for which the synthesis procedure was the same.

The synthesis process described above involves soaking the sample in acidic solution. Therefore the raw clay was also treated in acidic solution to check the influence of acid on the clay. A sample of raw clay was dispersed in HCl solution (pH = 0.8) and stirred at 50 °C for 3 h (the same as the acid treatment in the synthesis of the pillared clay), followed by separation by centrifugation and washing with water, drying

Table 1 Structural parameters of the raw clay and the TiO_2 pillared clays prepared

Sample[a]	Hydrothermal treatment conditions	Crystallite size of TiO_2[b] /Å	Average pore diameter[c] /Å	Total pore volume[c] /$cm^3\ g^{-1}$	Specific surface area[d] /$m^2\ g^{-1}$	Accessible surface area of TiO_2[e] /$m^2\ (g\ TiO_2)^{-1}$	TiO_2 Content[f] (wt%)
HT(200, 1)	200 °C,1 h	40	40	0.256	259	100.8	49.1
HT(200, 2)	200 °C,2 h	45	43	0.254	235	104.0	56.2
HT(200, 6)	200 °C,6 h	50	52	0.272	210	—[j]	43.1
HT(200, 24)	200 °C,24 h	77	69	0.256	181	81.0	47.6
HT(250, 2)	250 °C,2 h	55	55	0.287	208	—[j]	47.5
HT(250, 6)	250 °C,6 h	80	69	0.292	170	—[j]	45.9
HT(250, 24)	250 °C,24 h	90	81	0.286	141	73.3	36.3
UT-1[g]	untreated	—	34	0.216	256	72.5	47.7
UT-2[g]	untreated	—	37	0.221	241	86.0	51.2
RawClay-U[h]	—	—	158	0.083	21	—	—
RawClay-A[i]	—	—	99	0.098	40	—	—

[a]Samples were calcined at 500 °C. [b]Calculated from the (101) diffraction peak of anatase using the Scherrer equation. [c]Determined from nitrogen adsorption isotherms [d]Calculated from nitrogen adsorption isotherms using the BET equation. [e]Determined by a benzaldehyde–ammonia titration method.[19] [f]Determined by elemental analysis using the X-ray fluorescence method. [g]The preparation batch was the only difference between UT-1 and UT-2. [h]The raw clay untreated. [i]The raw clay treated in acid. [j]Not measured.

and heating at 500 °C. The untreated raw clay and the raw clay treated in acidic solution will be referred to as RawClay-U and RawClay-A, respectively.

Characterization

X-Ray diffraction (XRD) patterns were recorded by using a diffractometer with Cu tube (Rigaku Corporation, RAD-B). The specimens were prepared by spreading the wet sample on a glass slide and drying in air, followed by heating at 500 °C. Therefore, the silicate layers of the sample were oriented on the glass surface. The crystallite size of the TiO_2 pillars was calculated from the integral width of the anatase (101) diffraction peak ($2\theta = 25.3°$) using the Scherrer equation. In the calculation, the anatase (101) diffraction peak was separated from the background and a neighboring diffraction peak using the pattern decomposition method,[17] and 0.162 of the instrumental width at $2\theta = 25.3°$ was used from the calibration curve obtained from the measurement of silicon powder (Standard Reference Material, NIST).

Transmission electron microscopy (TEM) observations were performed by using a 200 kV instrument (JEOL Ltd., JEM-2010). The specimen was prepared by fixing the sample calcined at 500 °C in epoxy resin, followed by slicing *via* ultramicrotomy.

Nitrogen adsorption–desorption isotherms of the samples calcined at 500 °C were obtained at 77 K (Quantachrome Corporation, Autosorb-1). BET surface areas, total pore volumes, average pore diameters and pore size distribution curves were calculated from the isotherms. The average pore diameter was obtained using a cylindrical pore model. The pore size distribution curves were calculated by the Cranston–Inkley method[18] from the adsorption isotherms.

A benzaldehyde–ammonia titration method[19] (BAT) was used for measuring the accessible surface area of TiO_2 pillars in the pillared clay samples calcined at 500 °C. First, benzaldehyde was adsorbed on the surface of TiO_2 to form benzoate anions. It was confirmed in a separate experiment that benzaldehyde was not adsorbed on the surface of the montmorillonite. Then, ammonia was introduced to react with the benzoate anions to form benzonitrile. The density of benzoate adsorbed was obtained from the amount of benzonitrile formed, and the accessible surface area of the TiO_2 pillars was calculated by converting the density of benzoate on the pillared clay using the density on standard TiO_2.

The chemical compositions of the samples were determined by elemental analysis using the X-ray fluorescence method (Rigaku Industrial Corporation, RIX-2000). The samples calcined at 500 °C were dried at 120 °C and heated at 1100 °C. The ignition loss was obtained by weighing from 120 to 1100 °C. The specimens were prepared with the glass bead method.

UV absorption spectral measurements

UV absorption spectra of the samples calcined at 500 °C were measured by the diffuse reflection method using a spectrophotometer (Hitachi Ltd., U-3410) equipped with an integrating sphere of 60 mm diameter.

Elution of Ti in acidic solution

The samples calcined at 500 °C were used for these experiments. 20 mg of the sample was dispersed in 10 ml of HCl solution (pH 2–4) in a capped glass bottle, and then incubated at 50 °C for 6–144 h. The top layer of the solution was gathered and filtered with a membrane filter. The Ti concentration in the solution was determined by ICP spectrometry (Seiko Instruments Incorporated, SPS-1500VR). The amount of Ti eluted was defined as the weight ratio of Ti in the solution to the Ti in the original sample.

Photocatalytic degradation of trichloroethylene

The samples calcined at 500 °C were used for the photocatalysis experiments. The experimental cell was an Erlenmeyer flask made of borosilicate glass with a capacity of 30 ml. 25 ml of an aqueous solution of trichloroethylene (concentration 90 ppm) and 10 mg (in TiO_2 base) of the sample were placed in the flask and stirred with a magnetic stirrer. The UV irradiation was carried out with a xenon lamp shining through a borosilicate glass cell filter through which water was passed. The experiment was carried out at room temperature. The solution was extracted with a micro syringe through a rubber cap with which the flask was sealed, and the concentration of trichloroethylene was determined by gas chromatography (Shimadzu Corporation, GC-14A with a fused silica capillary column, Supelco Inc., SPB-5 at 40 °C with helium carrier gas).

Results

X-Ray diffraction

Fig. 1 shows the XRD patterns in the small-angle range of the raw clay (RawClay-U) and various TiO_2 pillared clay samples calcined at 500 °C. The specimens for XRD were prepared with the silicate layers oriented, thus the (00*l*) diffraction peak of the clay is emphasized and the other diffraction peak is weakened. RawClay-U showed the (001) diffraction peak at $2\theta = 6.9°$, as

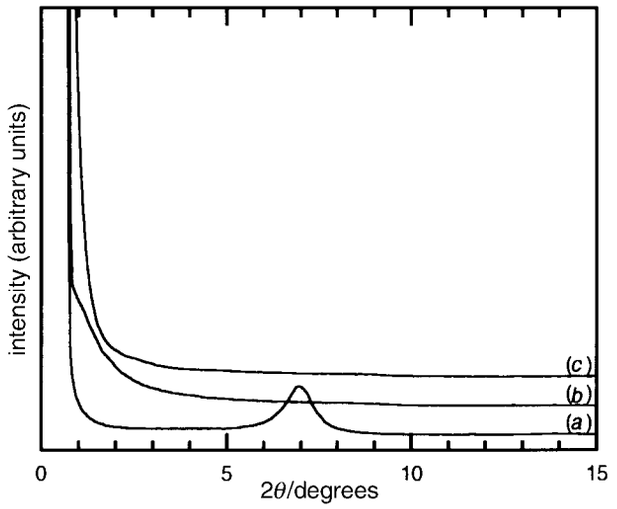

Fig. 1 XRD patterns of RawClay-U calcined at 500 °C (*a*), UT-1 calcined at 500 °C (*b*), and HT(200, 1) calcined at 500 °C (*c*).

shown in Fig. 1(*a*). On the other hand, the pillared clay samples, both untreated [UT-1, Fig. 1(*b*)] and hydrothermally treated [HT(200, 1), Fig. 1(*c*)], did not show the (001) peak, but small angle scattering was observed. These results show that the pillared clay samples did not have a sufficiently ordered and oriented silicate layer structure to show the (001) peak. The small angle scattering appeared at lower angles (near $2\theta<2°$) for HT(200, 1) than for UT-1 (near $2\theta=1$–$3°$). These results indicate that the mesopores are included in the pillared clays and that the hydrothermally treated sample has a larger pore size than the untreated one.

Fig. 2 shows the wide-angle XRD patterns of the pillared clays prepared under various treatment conditions. In Fig. 2(*a*), UT-1 dried at 120 °C did not show any peaks due to anatase. The XRD patterns of UT-1 heated at 500 °C [Fig. 2(*b*)] and at 600 °C [Fig. 2(*c*)] were almost the same and showed a broad and very weak peak due to the anatase phase at around $2\theta=25°$. However, the hydrothermally treated sample [HT(200,1), Fig. 2(*d*)] showed a more intense and sharper anatase peak than UT-1. Hydrothermal treatment under harsher conditions resulted in a sharper peak at $2\theta=25°$ and in additional anatase peaks becoming visible at $2\theta=48$, 55 and 63° [HT(250, 24), Fig. 2(*e*)]. These results indicate that the TiO_2 pillars are crystallized to anatase much better by the hydrothermal treatment than by calcination, and that the anatase crystallite size increases under prolonged hydrothermal treatment. The latter is more clearly shown by the squares in Fig. 3 which show the change in the TiO_2 crystallite size with hydrothermal treatment time. As the hydrothermal treatment time was extended, the TiO_2 size increased. In Fig. 2(*e*), HT(250, 24) exhibits two diffraction peak at $2\theta=21$ and 28°, besides the peaks due to anatase. These two peaks were also observed in the XRD pattern of HT(250, 6). The peaks could not be identified; they may be due to impurities (probably quartz) included in the raw clay or a secondary product formed during the more severe hydrothermal treatment.

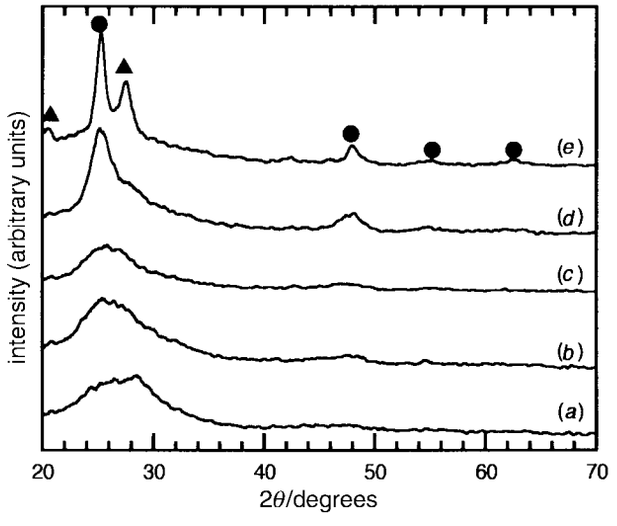

Fig. 2 XRD patterns of UT-1 dried at 120 °C (*a*), UT-1 calcined at 500 °C (*b*), UT-1 calcined at 600 °C (*c*), HT(200, 1) calcined at 500 °C (*d*), and HT(250, 24) calcined at 500 °C (*e*). ● and ▲ represent the diffraction peaks of anatase and unknown phases, respectively.

Transmission electron microscopy

Fig. 4(A) and (B) show TEM photographs of untreated (UT-2) and hydrothermally treated [HT(200, 6)] pillared clays, respectively. In the case of UT-2 shown in Fig. 4(A), the lines of the silicate layers are running from the upper left to the bottom right, and the silicate layers are oriented rather well, but are also partially disordered. In the case of the HT sample shown in Fig. 4(B), on the other hand, the lines of the silicate layers are running almost vertical, and the oriented state of the silicate layers is disordered in comparison with that of UT-2. The dark dots in the silicate interlayer in both TEM images are TiO_2 pillars. The darker dots in the HT sample compared to the UT sample may be due to the higher crystallinity of the TiO_2 pillars in the HT sample. The size distribution of the dots was also different between the UT and HT samples. In the case of UT-2 shown in Fig. 4(A), the distribution seems to be rather uniform, while the size of the dark dots in Fig. 4(B), *i.e.* TiO_2 pillars, in HT(200, 6) varies widely. It seems that the disorder of the silicate layers and the size distribution of the pillars is caused by the hydrothermal treatment.

Nitrogen adsorption

Fig. 5(A) shows adsorption–desorption isotherms of nitrogen on the raw clay (RawClay-U) and the raw clay treated in acid (RawClay-A). The adsorption isotherm of RawClay-U was near to type III, characteristic of a non-porous or macroporous solid in BDDT classification.[20] The desorption isotherm of RawClay-U showed slight hysteresis. It seems that this hysteresis resulted from the space between neighboring grains of the raw clay. RawClay-A showed larger hysteresis than RawClay-U. In Table 1, which shows the structural parameters of the samples obtained from the isotherms, RawClay-A displays a slightly larger specific surface area

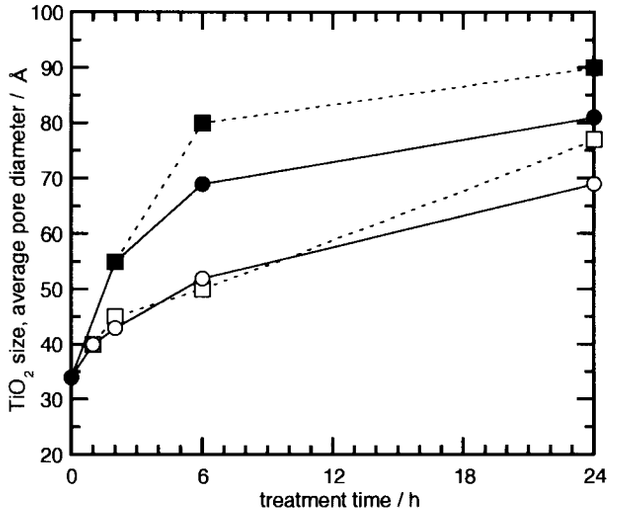

Fig. 3 Effect of hydrothermal treatment time on TiO_2 crystallite size (□, ■) and average pore diameter (○, ●) of pillared clay treated at 200 °C (○, □) and 250 °C (●, ■).

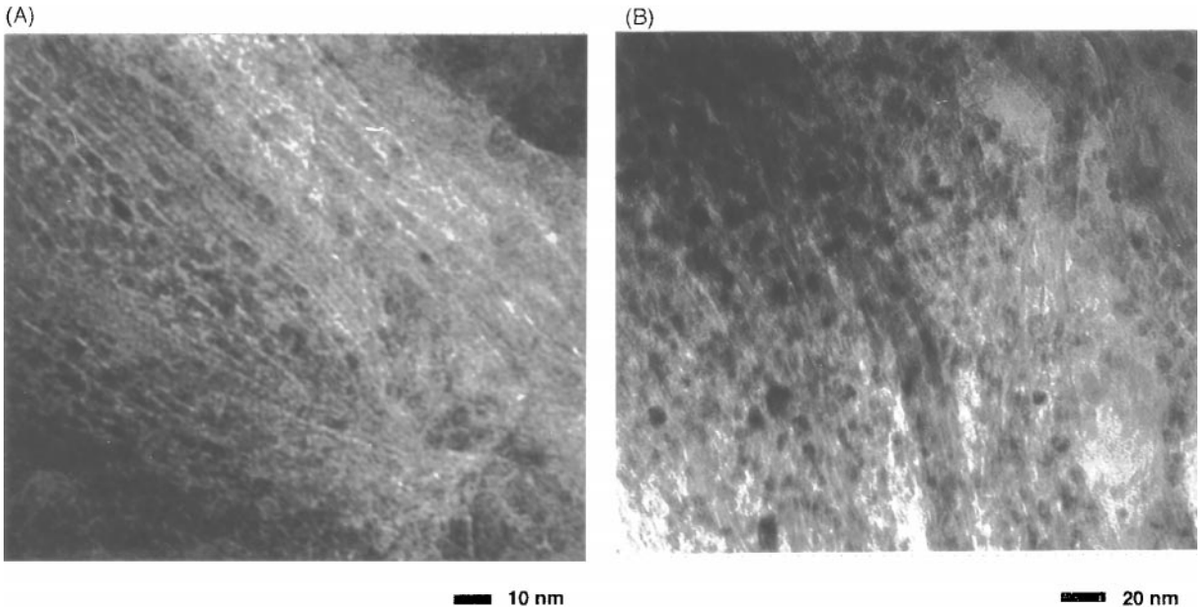

Fig. 4 TEM photographs of UT-2 calcined at 500 °C (A) and HT(200, 6) calcined at 500 °C (B).

and total pore volume than RawClay-U. These results indicate that RawClay-A possesses more developed porosity and, in particular, a larger mesopore volume than RawClay-U. This mesopore volume seems to be due to the delaminated structure[21,22] formed in the raw clay upon acid treatment. From the data in Table 1, RawClay-A shows a smaller average pore diameter than RawClay-U, which indicates that the size of the pores in the delaminated structure in RawClay-A is smaller than that with spaces between neighboring grains in RawClay-U.

Fig. 5(B) shows the adsorption–desorption isotherms of nitrogen on the hydrothermally treated [HT(200, 1)], [HT(250, 24)] and untreated (UT-1) pillared clays and RawClay-A. In Fig. 5(B) and the adsorption isotherms of the pillared clays do not show any clear bending caused by monomolecular layer adsorption at nearly zero relative pressure. This result seems to be caused by lower degassing efficiency in the instrument; monomolecular layer adsorption *was* shown in adsorption isotherms of the pillared clays measured with another instrument for which the degassing efficiency was higher. Therefore, the isotherms of the pillared clays seem to be nearly type IV, characteristic of solids containing both micro- and meso-pores (BDDT classification).[20] The amounts of N_2 sorbed on the pillared clays were very much larger than that on RawClay-A, which indicates that the porous structure was largely developed by pillaring. The adsorption isotherms on

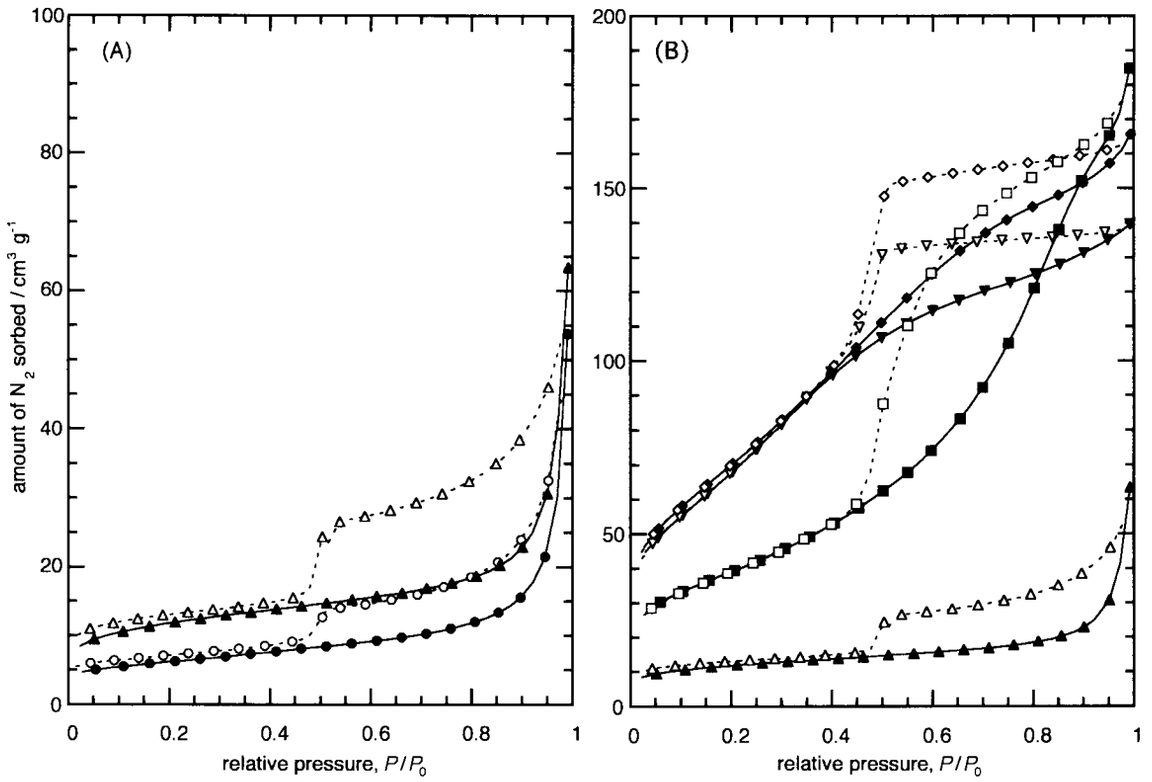

Fig. 5 Adsorption–desorption isotherms of nitrogen [(A) and (B)] on RawClay-U (●, adsorption; ○, desorption), RawClay-A (▲, adsorption; △, desorption), UT-1 (▼, adsorption; ▽, desorption), HT(200, 1) (◆, adsorption; ◇, desorption) and HT(250, 24) (■, adsorption; □, desorption).

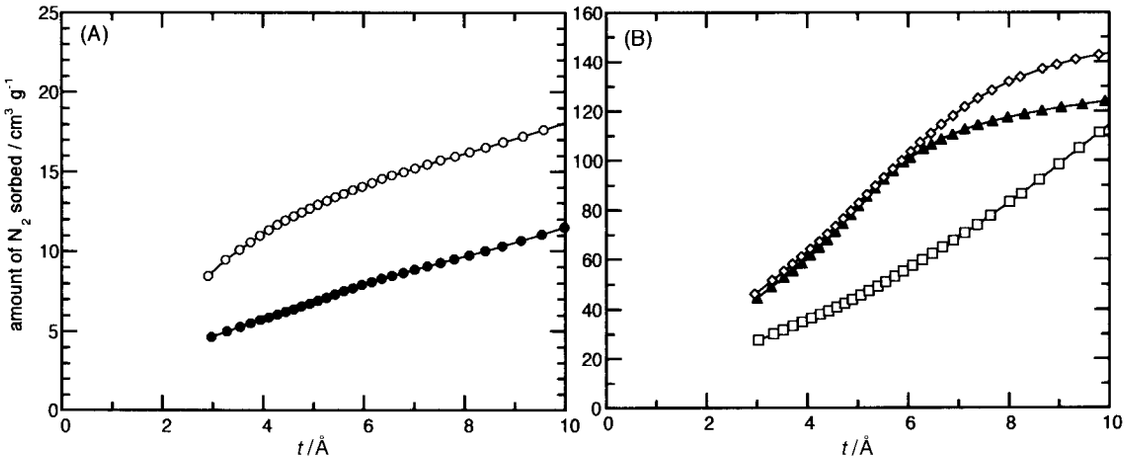

Fig. 6 *t*-Plots [(A) and (B)] of RawClay-U (●), RawClay-A (○), UT-1 (▲), HT(200, 1) (◇) and HT(250, 24) (□).

pillared clays fitted the BET equation for the relative pressure range 0.05–0.30. Of the pillared clays, HT(200, 1) adsorbed a larger amount of N_2 than UT-1 for relative pressures over 0.4, which indicates that HT(200,1) possesses more volume in the mesopore region than UT-1. HT(250, 24) showed a gentler slope of the adsorption isotherm for relative pressures below 0.3 than HT(200, 1), and a steeper slope for relative pressures >0.4. This indicates that HT(250, 24) hydrothermally treated under more severe conditions possesses a smaller micropore volume and a larger mesopore volume than HT(200, 1) treated under milder conditions.

In Table 1, the increases in specific surface area and total pore volume of RawClay-A compared with RawClay-U were small. Therefore, it is considered that the formation of the delaminated structure with acid treatment in the synthesis process was partial in RawClay-A and probably in the pillared clays as well. Comparison of the pillared clays with the raw clay samples shows that the specific surface area and total pore volume were increased greatly. Fig. 6 shows *t*-plots[23] of the raw clay samples (RawClay-U and RawClay-A) and the pillared clay samples [UT-1, HT(200, 1) and HT(250, 24)]. The *t*-plots of RawClay-A UT-1 and HT(200, 1) shown can be extrapolated to the origin and have a bending point. This type of *t*-plot is characteristic of porous solids possessing both micro- and mesopores and can be analyzed to obtain micropore parameters. RawClay-U and HT(250, 24) did not show clear bending on their *t*-plots. The *t*-plot of RawClay-U was almost a straight line which was extrapolated to the ordinate to obtain a positive intercept. This type of *t*-plot is characteristic of solids possessing only micropores. HT(250, 24) showed a *t*-plot which could be extrapolated to the origin. This type of *t*-plot is characteristic of solids possessing only mesopores. The *t*-plot of HT(250, 24) is curved upwards. This curve seems to be due to capillary condensation in mesopores. Table 2 shows micropore parameters obtained from analysis of the *t*-plots (Fig. 6). The pillared clay samples [UT-1 and HT(200, 1)] showed much larger micropore parameters than RawClay-A. The silicate layers of the pillared clay synthesized in acidic solution seemed to form a delaminated structure as RawClay-A showed more developed porosity than RawClay-U (Table 1). However, in Tables 1 and 2, the large increase in the parameters in the porous structure for the pillared clay samples compared to the raw clay samples cannot be accounted for solely by the formation of the delaminated structure. Therefore, it is considered that the delaminated structure contributed a little to the porosity of the pillared clay samples and that TiO_2 was indeed intercalated into the silicate layers of the clay and exists as pillars in the samples.

Fig. 7 shows the changes in BET surface area and total pore volume with hydrothermal treatment time. As both the treatment time and treatment temperature increased, the BET surface area decreased and the total pore volume increased.

The circles in Fig. 3 show the changes in the average pore diameter for pillared clays with hydrothermal treatment time. The average pore diameter showed good agreement with the TiO_2 pillar size calculated from XRD, and it increased as the hydrothermal treatment time was increased and the treatment temperature was raised. Therefore, it seemed that the average

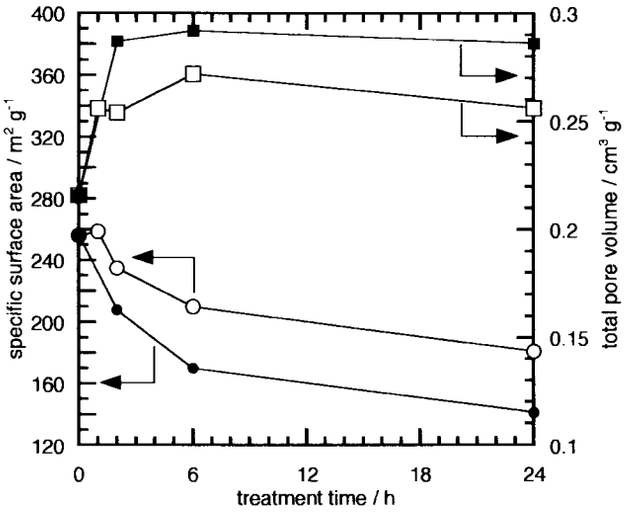

Fig. 7 The changes in BET surface area (○, ●) and total pore volume (□, ■) with hydrothermal treatment at 200 °C (○, □) and at 250 °C (●, ■).

Table 2 Micropore parameters obtained from *t*-plot analysis[22]

Sample	Inner surface area of micropores/m^2 g^{-1}	Inner volume of micropores/cm^3 g^{-1}	External surface area of micropores /m^2 g^{-1}	Diameter of micropores/Å
RawClay-A	25	0.013	15	8.8
UT-1	204	0.140	52	13.6
HT(200, 1)	166	0.129	93	15.6

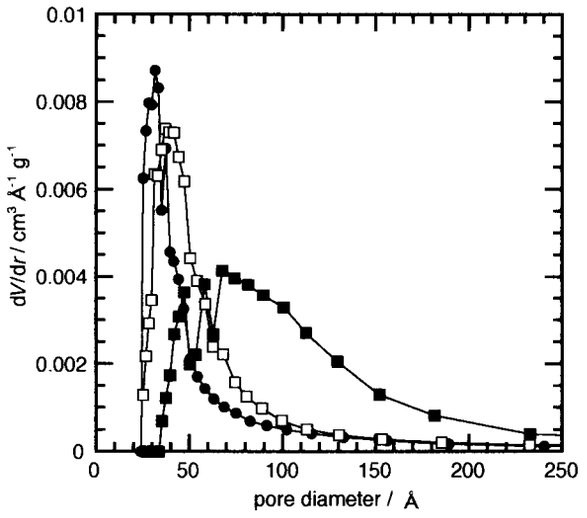

Fig. 8 Pore size distribution curves of UT-1 (●), HT(200, 1) (□) and HT(250, 24) (■).

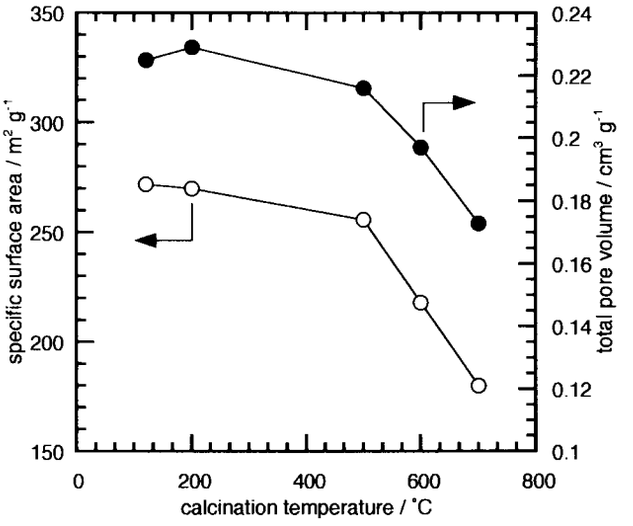

Fig. 9 The changes in BET surface area (○) and total pore volume (●) of UT-1 with calcination temperature.

pore diameter could be substituted for the TiO_2 pillar size or interlayer distance of the pillared clay. Fig. 8 shows the pore size distribution curves of the pillared clay samples [UT-1, HT(200, 1) and HT(250, 24)]. As the hydrothermal treatment conditions became more severe, the curve shifted to larger pore sizes and the shape of the curve was broadened. The pore diameter giving the maximum in the pore size distribution curve also showed good agreement with the average pore diameter and the TiO_2 pillar size (Table 1 and Fig. 3).

Fig. 9 shows changes in the BET surface area and the total pore volume of untreated TiO_2 pillared clay (UT-1) with the calcination temperature. In this case, both the BET surface area and the total pore volume were markedly reduced at 600 °C or more. Thus, the porous structure of the pillared clay was destroyed upon calcination at temperatures above 600 °C. Therefore, in this study, the calcination temperature of the pillared clay samples was set at 500 °C in the synthesis process.

Benzaldehyde–ammonia titration

Fig. 10 shows the relationship between the TiO_2 pillar size and the accessible surface area of TiO_2 pillars, estimated by the BAT method. The TiO_2 pillar sizes were estimated from the TiO_2 crystallite size and the average pore diameter in Table 1. The dotted curve in Fig. 10 represents the specific surface area of anatase particles calculated by assuming spherical particles, and the solid curve represents the accessible surface area of anatase pillars by assuming cubic particles with four faces exposed. In the calculation of both curves, the density of anatase (3.84 g cm^{-3})[24] was used. The accessible surface areas were considerably smaller than the calculated curves, and the ratio of accessible surface area to calculated value decreased with decreasing TiO_2 pillar size. The accessible surface area of the HT samples was found to decrease with increasing TiO_2 pillar size upon hydrothermal treatment. The accessible surface area of the UT samples was smaller than that expected from the correlation curve of the HT samples. These results indicate that the hydrothermal treatment increased the ratio of accessible surface area to total surface area of TiO_2 pillars, probably as a result of the developing porous structure of the pillared clay.

Chemical composition

In Table 1, the TiO_2 content of the prepared pillared clays, except HT(250, 24), ranged from 43.1 to 56.2 wt%. These values were similar to those from previously published studies.[10,11,13,14] HT(250, 24), in particular, showed a lower

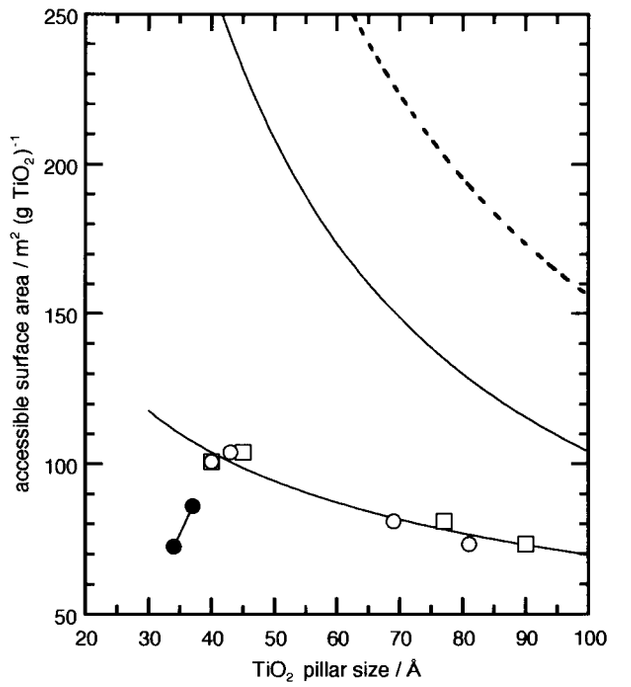

Fig. 10 Relationship between the accessible surface area of TiO_2 pillars and their size for untreated (●) and hydrothermally treated (○, □) samples. TiO_2 pillar size was estimated from the average pore diameter (●, ○) and the TiO_2 crystallite size (□). The dotted curve represents the specific area of anatase particles calculated by assuming spherical particles, and the solid curve represents the accessible surface area of anatase pillars calculated by assuming cubic particles with four faces exposed (the upper and lower faces are not exposed).

TiO_2 content than the other prepared pillared clays. This result seems to indicate that Ti was eluted from the pillared clay under the most severe hydrothermal treatment conditions.

Table 3 shows the chemical compositions of raw clay (RawClay-U) and TiO_2 pillared clay samples [UT-1, HT(200, 1) and HT(250, 24)]. The pillared clays were treated in acidic solution during the synthesis process. Al, Mg and Fe are usually eluted from silicate clay layers upon acid treatment. But, in Table 3, the Al/Si, Mg/Si and Fe/Si values for the pillared clays [UT-1, HT(200, 1) and HT(250, 24)] did not decrease compared with the raw clay (RawClay-U). Thus, elution of metal from the silicate layers was minimal in the

Table 3 Chemical composition of the raw clay and the TiO_2 pillared clays prepared

Metal oxide content[a] (wt%)	Sample[b]			
	RawClay-U	UT-1	HT(200, 1)	HT(250, 24)
SiO_2	60.4	31.4	29.8	37.0
Al_2O_3	23.9	12.0	12.3	15.3
MgO	3.5	1.7	1.5	2.1
Fe_2O_3	2.0	1.0	1.0	1.3
CaO	0.5	—	—	—
Na_2O	2.8	0.4	0.4	0.4
K_2O	0.1	0.2	0.3	0.2
TiO_2	—	47.7	49.1	36.3
H_2O[c]	5.8	5.5	5.5	4.6
Total	99.0	99.9	99.9	97.2
Al/Si[d]	0.47	0.45	0.49	0.49
Mg/Si[d]	0.086	0.081	0.075	0.084
Fe/Si[d]	0.025	0.024	0.025	0.026
Ti/Si[d]	—	1.14	1.23	0.74

[a]Determined by elemental analysis using the X-ray fluorescence method. [b]Samples were calcined at 500 °C, and dried at 120 °C for weighing before analysis. [c]Ignition loss from 120 to 1100 °C. [d]Atomic molar ratio.

synthesis of the pillared clay samples, and the silicate layer of the pillared clay seemed to be hardly damaged by acidic or hydrothermal treatment.

UV absorption spectra

Fig. 11(A) shows UV-visible diffuse reflectance spectra of TiO_2 pillared clays [UT-1, HT(200, 1), HT(250, 24)] calcined at 500 °C in comparison with those of anatase, rutile and the raw clay (RawClay-U). The raw clay was almost transparent to UV for wavelengths longer than 300 nm. Therefore, the photocatalytic reaction in the interlayer space does not seem to be affected by any decrease in intensity of the UV rays as they pass through the silicate layers of the clay. The TiO_2 pillared clays, anatase and rutile showed an absorption edge in their reflectance spectra.

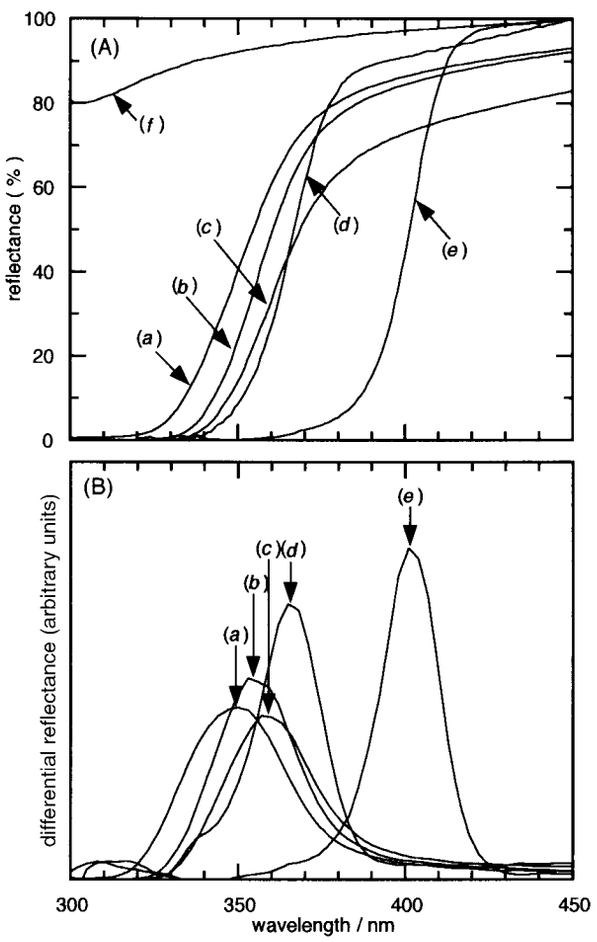

Fig. 11 UV-visible diffuse reflectance spectra (A) and UV-visible differential reflectance spectra (B) of UT-1 (*a*), HT(200, 1) (*b*), HT(250, 24) (*c*), anatase (*d*), rutile (*e*) and RawClay-U (*f*).

Fig. 11(B) shows differential reflectance spectra obtained by differentiating the ordinate of the spectra in Fig. 11(A). The absorption edges of the TiO_2 pillared clays were blue-shifted in comparison with that of anatase, and were shifted toward shorter wavelengths, as the TiO_2 pillar size or the average pore diameter (Table 1) became smaller.

Elution test of TiO_2 pillars in acidic solution

Fig. 12 shows a comparison of the durability of the TiO_2 pillars in HCl solution between hydrothermally treated [HT(200, 1)] and untreated (UT-2) samples. The TiO_2 pillar size of [HT(200, 1)] and the average pore diameter of UT-2 (Table 1) are almost equal. In pH 4 solution, the elution of Ti from HT(200, 1) could not be observed until after 144 h of reaction, but UT-2 showed a little elution at 144 h. In pH 2 solution, both samples showed the elution of Ti, but UT-2 clearly showed more elution than HT(200, 1). Thus, it was demonstrated that the crystallization of TiO_2 pillars by hydrothermal treatment improves their durability in acidic solution.

Photocatalytic degradation of trichloroethylene

Fig. 13 shows a comparison of the photocatalytic activity between the hydrothermally treated [HT(200, 1)] and untreated (UT-2) samples. The TiO_2 pillar size of [HT(200, 1)] and the average pore diameter of UT-2 (Table 1) are almost equal. As shown, trichloroethylene degradation fitted a first order rate expression, and HT(200, 1) clearly lowered the trichloroethylene concentration faster than UT-2.

Fig. 14(A) shows the effect of the TiO_2 pillar size on the pseudo-first order reaction rate constant of trichloroethylene degradation per unit weight of TiO_2. The TiO_2 pillar sizes were estimated from the TiO_2 crystallite size and the average pore diameter in Table 1. As shown, in the case of the HT samples, the rate constant increased with decreasing TiO_2 pillar size. The rate constants of the UT samples did not agree with this correlation curve for HT samples, and they were considerably smaller than the values expected from the curve.

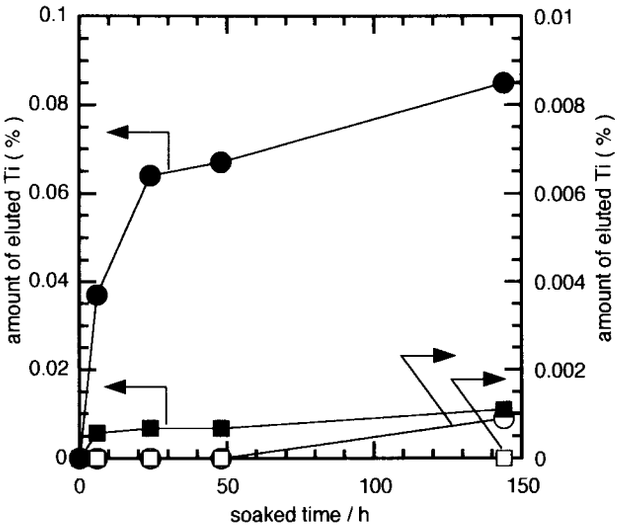

Fig. 12 Amount of Ti eluted from UT-2 (●, ○) and HT(200, 1) (■, □) samples in HCl solutions of pH 2 (●, ■) and pH 4 (○, □) at 50 °C.

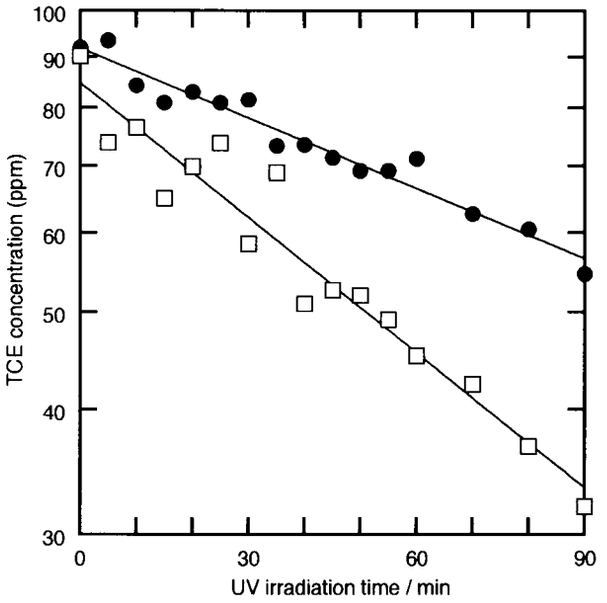

Fig. 13 Decrease of trichloroethylene (TCE) concentration in photocatalytic degradation over UT-2 (●) and HT(200, 1) (□).

Fig. 14(B) shows the pseudo-first order reaction rate constants per accessible unit surface area of the TiO_2 pillars. The variation of the reaction rate constant with varying TiO_2 pillar size was smaller than that shown in Fig. 14(A), because the accessible surface area increased with decreasing pillar size as shown in Fig. 10. Although the difference in the activity between UT samples and HT samples was also smaller for the same reason, the activity of UT samples was still lower than the correlation curve for HT samples.

Discussion

Structure of silicate layers

In the N_2 adsorption measurements (Fig. 5 and Table 1), a large increase in porosity was shown for the pillared clay samples in comparison with the raw clay. The causes for this increasing porosity are considered to be the formation of the delaminated structure and the pillaring of TiO_2. The delaminated structure formation seems to be a minor cause, because the increase in porosity for the delaminated structure was small in both the micro- and meso-pore regions (Fig. 5, 6 and Tables 1, 2). From this result, it is considered that the formation of the delaminated structure was partial in the pillared clays. From the structure of the delaminated clay, pores formed with delamination are mainly macro- or meso-pore sized. On the other hand, the pillared clay samples showed high porosity in both the micro- and meso-pore regions (Fig. 5, 6 and Tables 1, 2). From these results, especially from the high microporosity of the pillared clay samples, pillaring seems to be the major cause of increased porosity.

In the TEM photographs (Fig. 4) which showed the local structure of the pillared clays, reasonably well-oriented structure of the silicate layers and also partial disorder of the layers were observed. In the small angle XRD patterns (Fig. 1), the pillared clays did not show the (001) diffraction peak, only small angle scattering. Therefore, the oriented structure of the silicate layers was not sufficiently well ordered to exhibit the (001) diffraction peak. One cause of disorder in the oriented silicate structure seems to be the size distribution of the

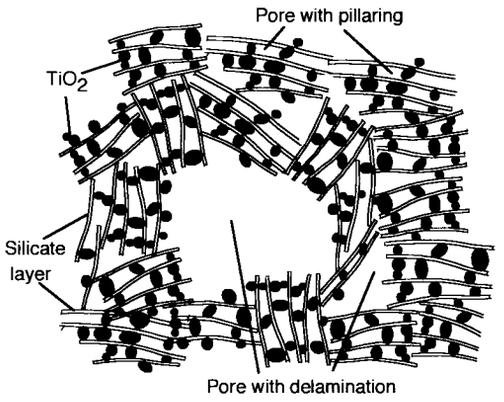

Fig. 15 Schematic structural model of the TiO_2 pillared clay prepared.

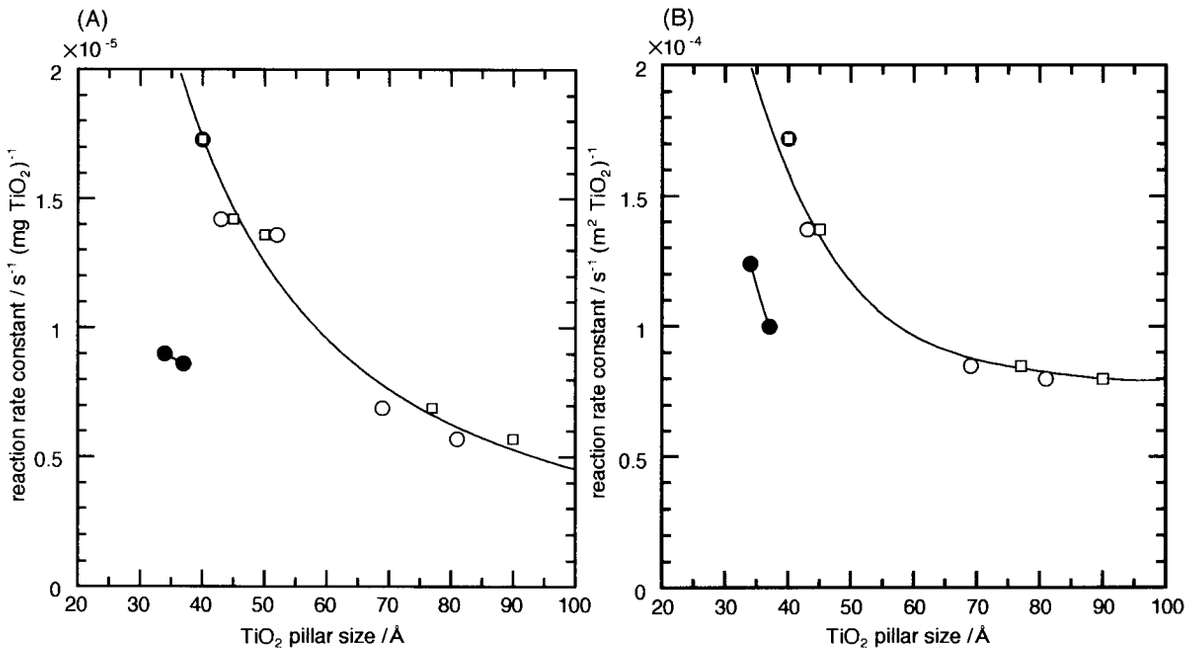

Fig. 14 The effect of TiO_2 pillar size on the reaction rate constant per unit weight of TiO_2 (A) and on the reaction rate constant per accessible until surface area of TiO_2 pillar (B) in photocatalytic degradation of trichloroethylene over untreated (●) and hydrothermally treated (○, □) samples. TiO_2 pillar size was estimated from average pore diameter (●, ○) and TiO_2 crystallite size (□).

precursor of the TiO_2 pillars. Yamanaka *et al.* showed that titanium hydroxopolycation particles in TiO_2 sols have a size distribution which changes with the extent of peptization of the sol.[11] Another cause of the disorder seems to be the partially delaminated structure.[21,22] A schematic structural model of the TiO_2 pillared clay prepared is shown in Fig. 15. This shows the disordered silicate layers with a wide size distribution of TiO_2 pillars and the mixture of partially delaminated and reasonably well-oriented structures.

Hydrothermally treated samples are considered to have larger interlayer distances than the untreated samples, because the former exhibited X-ray scattering at lower angles than the latter (Fig. 1). As the treatment time was lengthened and the treatment temperature raised, the total pore volume (Fig. 7) and the average pore diameter (Fig. 3) increased and the pore size distribution curve was shifted toward larger pore sizes (Fig. 8). However, there were side effects of the hydrothermal treatment process which resulted in decreased BET surface areas (Fig. 7), increased extent of disorder in the oriented silicate layers (Fig. 4) and broadened pore size distributions (Fig. 8).

It should be noted that the porous structure could be developed only by the hydrothermal treatment, and not by calcination of the pillared clay (Fig. 9).

In Fig. 2(*e*), the possible generation of a secondary product during the most severe hydrothermal treatment is indicated. Zeolites are microporous, crystalline materials which may potentially be generated by the hydrothermal treatment of a clay. However, the *t*-plot of the pillared clay hydrothermally treated under the most severe conditions [HT(250, 24)] did not show zeolitic microporosity [Fig. 6(B)]. Additionally, the chemical composition of HT(250, 24) was not markedly different from that of the untreated pillared clay (Table 3). From these results, even if zeolite was generated as a secondary product in the hydrothermal treatment, it would be produced in very small amounts which have little influence on the adsorption efficiency of the pillared clay, and such a small quantity of product in HT(250, 24) is unlikely to affect the photocatalytic properties.

Structure of TiO_2 pillars

Einaga suggested $[(TiO)_8(OH)_{12}]^{4+}$ as a titanium hydroxopolycation present in hydrochloric acid solution.[25] Supposing that all the cations in the interlayer spaces of the raw clay were exchanged with $[(TiO)_8(OH)_{12}]^{4+}$, the molar ratio of TiO_2/eq. of exchangeable cation in the raw clay would be 2. In the case of UT-1, the molar ratio of TiO_2/eq. of exchangeable cation in the raw clay was estimated as about 10 from the data in Table 3. From this result, we can deduce that the titanium hydroxopolycations in the prepared TiO_2 sol were larger species than $[(TiO)_8(OH)_{12}]^{4+}$. Yamanaka *et al.* showed that the size of the titanium hydroxopolycation changed with the extent of peptization of the sol.[11] In our case, the extent of peptization of the prepared sol seems insufficient to generate small species like $[(TiO)_8(OH)_{12}]^{4+}$.

In the pillared clays, it is possible that TiO_2 may exist both in the interlayer spaces and on the external surface of the pillared clay. The quantitative proportions of TiO_2 in these different sites are unknown. However, TiO_2 will exist mainly as pillars in the interlayer spaces, because the interlayer surface area is much larger than the external surface area of the raw clay. Additionally, the pillared clays showed large specific surface areas, total pore volumes and especially microporosity (Tables 1 and 2). These results indicate that a considerable quantity of TiO_2 was intercalated in the silicate layers in the pillared clays. To confirm this, the interlayer space of the pillared clay and the volume of TiO_2 pillars were estimated and compared. In the case of UT-1, the structural formula of anhydrous UT-1 was $(TiO_2)_{4.43}\cdot(Si_{3.89}Al_{0.11})(Al_{1.60}Fe_{0.08}Mg_{0.32})O_{10}(OH)_2$ from Table 3 and the structural formula of the raw clay.[16] The contents of each clay and TiO_2 in the pillared clay were calculated from the structural formula of the pillared clay. The interlayer space was calculated to be: clay content × inner surface area of clay × 0.5 × interlayer distance. The volume of TiO_2 pillars was calculated to be: TiO_2 content/density of TiO_2. Using 800 $m^2\ g^{-1}$ as the inner surface area of montmorillonite[26] and 34 Å as the interlayer distance of UT-1 (substituted with the average pore diameter in Table 1), the interlayer space in UT-1 was estimated as 0.7 $cm^3\ g^{-1}$. Using 3.84 g cm^{-3} as the density of TiO_2 (substituted with the value for anatase[24]), the volume of TiO_2 pillars in UT-1 was estimated as 0.1 $cm^3\ g^{-1}$. Therefore, the interlayer space of the pillared clay was enough to intercalate TiO_2 of about 50 wt% of the sample.

The XRD (Fig. 2) and N_2 adsorption results (Fig. 9) indicate that TiO_2 pillars can not be crystallized with retention of the porosity of the pillared clay upon calcination. This is because the TiO_2 pillars were only poorly crystallized even with calcination at 600 °C, which resulted in the destruction of the porous structure of the pillared clay. On the other hand, the hydrothermal treatment *is* effective for the crystallization of TiO_2 pillars with retention of the porosity of the pillared clay. With hydrothermal treatment, TiO_2 pillars were crystallized to anatase well (Fig. 2) and the total pore volume was increased (Fig. 7). The TiO_2 crystallite size can be changed by altering the hydrothermal treatment conditions: the TiO_2 size increased as hydrothermal treatment time was lengthened and the treatment temperature was raised (Fig. 3).

On the other hand, the hydrothermal treatment resulted in a non-uniform distribution of TiO_2 pillar size in comparison with the untreated samples (Fig. 4) as well as the increased disorder of the silicate layers (Fig. 4), broadening of the pore size distribution (Fig. 8) and decreasing BET surface area (Fig. 7). These results may be explained by Ostwald ripening,[27] namely, the pillar growth proceeds through a process of dissolution of relatively small TiO_2 pillars in water, followed by re-deposition on relatively large pillars. This may result not only in the broadening of the distribution of TiO_2 pillar size but also the enlargement of pores alongside the growing pillar. This supposition is supported by the close agreement between the TiO_2 crystallite size obtained from XRD with the average pore diameter (Fig. 3), which means that the pore size is determined by the size of the TiO_2 pillars. Such changes in pore structure may cause the disorder of the silicate layers (Fig. 4), the broadening of the pore size distribution (Fig. 8) and the decrease in BET surface area (Fig. 7). The increase in the ratio of accessible surface area of TiO_2 pillars to calculated surface area (Fig. 10) may also be caused by the enlargement of pores containing TiO_2 pillars.

Catalytic properties of hydrothermally crystallized TiO_2 pillars

In the present study, the TiO_2 pillars in the interlayer spaces of montmorillonite were found to function as a photocatalyst for the photodegradation of trichloroethylene in water, as well as the photodegradation of dibutylphthalate in water.[28] As shown in Fig. 14, the TiO_2 pillar size had a large effect on the photocatalytic activity both per unit weight of TiO_2 and per accessible unit surface area of TiO_2. In particular, the effect on the photocatalytic activity per accessible unit surface area of TiO_2 indicated that the photocatalytic activity was influenced by other factors as well as the change in surface area of the TiO_2 pillars. The photocatalytic activity increased with decreasing TiO_2 pillar size from 90 to 40 Å, which was accompanied by a blue-shift of the absorption edge in the UV spectrum (Fig. 11). These results seem to indicate the appearance of a quantum-size effect. This is because the blue-shift of the optical band edge was interpreted previously as a quantum-size effect,[12,15,29] and because this effect has been

confirmed to arise in the photocatalytic activity of TiO_2 particles of size <100 Å.[30] Although the quantum-size effect is not directly related to the increasing photocatalytic activity, an enhancement of the photocatalytic activity was often experienced when the absorption spectra were shifted to the higher energy region.[15,29,30] Our case of photodegradation of trichloroethylene with TiO_2 can also be classified as an example which is enhanced by the quantum-size effect.

The photocatalytic activity can be further improved by the crystallization of TiO_2 pillars. Although the untreated sample (UT-1, TiO_2 pillar size estimated as 34 Å from the average pore diameter in Table 1) showed a larger blue-shift than the hydrothermally crystallized sample [HT(200, 1), TiO_2 pillar size 40 Å from Table 1] in Fig. 11, the photocatalytic activity of the former was lower than that of the latter (Fig. 14). Therefore, hydrothermal crystallization is considered to have a greater influence on the photocatalytic activity than the quantum-size effect.

The hydrothermal crystallization of TiO_2 pillars also resulted in their increased durability in acidic solution compared with untreated samples (Fig. 12). The durability is an important factor for the application of TiO_2 pillared clays as photocatalysts for the decomposition of toxic substance containing halogens in water, because the solution is considered to become acidic as decomposition proceeds.

From these results, the hydrothermal crystallization was recognized to improve the photocatalytic activity and durability of TiO_2 pillars.

Conclusions

A pillared montmorillonite with crystallized TiO_2 was developed as a new type of pillared clay, and the following conclusions were made regarding its structure and photocatalytic properties.

(1) TiO_2 pillars in pillared montmorillonite could be crystallized to anatase by hydrothermal treatment, while the porosity of the pillared clay was retained.

(2) The size of the crystallized TiO_2 pillars and the average pore diameter showed good agreement, and both sizes could be controlled in the range *ca.* 40–90 Å by changing the treatment conditions.

(3) As the TiO_2 pillar size became small, the pillared montmorillonite exhibited higher catalytic activity, in the photocatalytic degradation of trichloroethylene in water, due to the quantum-size effect, which was confirmed by blue-shifts in the UV spectra.

(4) The hydrothermal crystallization had a greater influence on the photocatalytic activity than the quantum-size effect: the hydrothermally crystallized TiO_2 pillars showed higher photocatalytic activity than the untreated amorphous pillars, although the crystallized pillars showed a smaller blue-shift than the amorphous pillars.

(5) The hydrothermal crystallization of TiO_2 pillars was effective for the improvement of their durability in acidic solution: the hydrothermally treated TiO_2 pillared montmorillonite showed lower elution of Ti into HCl solution than the untreated sample.

References

1 G. W. Brindley and R. E. Sampels, *Clay Miner.*, 1977, **12**, 229.
2 T. J. Pinnavaia, *Science*, 1983, **220**, 365.
3 J. Shabtai, M. Rosell and M. Tokarz, *Clays Clay Miner.*, 1984, **32**, 99.
4 S. Yamanaka, *Am. Ceram. Soc. Bull.*, 1991, **70**, 1056.
5 M. L. Occelli, *J. Mol. Catal.*, 1986, **35**, 337.
6 F. Figueras, *Catal. Rev. Sci. Eng.*, 1988, **30**, 457.
7 E. Kikuchi and T. Matsushita, *Catal. Today*, 1988, **2**, 297.
8 M. Horio, K. Suzuki, H. Masuda and T. Mori, *Appl. Catal.*, 1991, **72**, 109.
9 P. Malla, S. Yamanaka and S. Komarneni, *Solid State Ionics*, 1989, **32/33**, 354.
10 J. Sterte, *Clays Clay Miner.*, 1986, **34**, 658.
11 S. Yamanaka, T. Nishihara, M. Hattori and Y. Suzuki, *Mater. Chem. Phys.*, 1987, **17**, 87.
12 S. Yamanaka and K. Makita, *J. Porous Mater.*, 1995, **1**, 29.
13 A. Bernier, L. F. Admaiai and P. Grange, *Appl. Catal.*, 1991, **77**, 269.
14 L. Khalfallah Boudali, A. Ghorbel, D. Tichit, B. Chiche, R. Dutartre and F. Figueras, *Microporous Mater.*, 1994, **2**, 525.
15 H. Yoneyama, S. Haga and S. Yamanaka, *J. Phys. Chem.*, 1989, **93**, 4833.
16 Data provided by Kunimine Industrial Company.
17 R. A. Young, E. Prince and R. A. Sparks, *J. Appl. Crystallogr.*, 1982, **15**, 357.
18 R. W. Cranston and F. A. Inkley, *Adv. Catal.*, 1957, **9**, 143.
19 M. Niwa, S. Inagaki and Y. Murakami, *J. Phys. Chem.*, 1985, **89**, 3869.
20 S. Brunauer, L. S. Deming, S. W. Deming and E. Teller, *J. Am. Chem. Soc.*, 1940, **62**, 1723.
21 T. J. Pinnavaia, M. Tzou, S. D. Landau and R. H. Raythatha, *J. Mol. Catal.*, 1984, **27**, 195.
22 M. L. Occeli, *Catal. Today*, 1988, **2**, 339.
23 J. H. de Boer, B. C. Lippens, B. G. Linsen, J. C. P. Broekhoff, A. van den Heuvel and Th. J. Osinga, *J. Colloid Interface Sci.*, 1966, **21**, 405.
24 G. V. Samsonov (ed.), *The Oxide Handbook*, IFI/Plenum, New York, 1973, p. 34.
25 H. Einaga, *J. Chem. Soc., Dalton Trans.*, 1979, 1917.
26 G. Sposito, *The Surface Chemistry of Soils*, Clarendon Press, Oxford and New York, 1984, p. 25.
27 H. E. Buckley, *Crystal Growth*, John Wiley & Sons, New York, 1951, p. 23.
28 H. Yoshida, T. Kawase, Y. Miyasita, C. Murata, C. Ooka and T. Hattori, *Chem. Lett.*, 1999, 715.
29 M. Anpo, N. Aikawa, Y. Kubokawa, M. Che, C. Louis and E. Giamello, *J. Phys. Chem.*, 1985, **89**, 5017.
30 M. Anpo, T. Shima, S. Kodama and Y. Kubokawa, *J. Phys. Chem.*, 1987, **91**, 4305.

Paper 9/01421G